



Laminar Flow Control and Drag Reduction using Biomimetically Inspired Forward Facing Steps

Dinesh Bhatia¹, Guangning Li², Jing Sun³, Jian Wang⁴

¹ School of Aerospace Engineering, The University of Nottingham Ningbo China, 199 Taikang East Road, Ningbo 315100, China, E-mail: Dinesh.Bhatia@nottingham.edu.cn

² School of Astronautics, Northwestern Polytechnical University, 127 Youyi West Road, Xi'an 710072, China, Email: lgning@nwpu.edu.cn

³ School of Aeronautics, Northwestern Polytechnical University, 127 Youyi West Road, Xi'an 710072, China, Email: sunjinglemon@nwpu.edu.cn

⁴ Faculty of Science, Engineering and Computing, Kingston University London, Friars Avenue, London SW15 3DW, United Kingdom, Email: J.Wang@kingston.ac.uk

Received September 18 2020; Revised November 22 2020; Accepted for publication December 17 2020.

Corresponding author: D. Bhatia (Dinesh.Bhatia@nottingham.edu.cn)

© 2020 Published by Shahid Chamran University of Ahvaz

Abstract. This paper explores the use of shark-skin inspired two-dimensional forward facing steps to attain laminar flow control, delay boundary layer transition and to reduce drag. Computation Fluid Dynamics (CFD) simulations are carried out on strategically placed forward facing steps within the laminar boundary layer using the Transition SST model in FLUENT after comprehensive benchmarking and validation of the simulation setup. Results presented in this paper indicate that the boundary layer thickness to step height ratio (δ/h), as well as the location of the step within the laminar boundary layer (x/L), greatly influence transition onset. The presence of a strategically placed forward facing step within the laminar boundary layer might damp disturbances within the laminar boundary layer, reduce wall shear stress and energize the boundary layer leading to transition onset delay and drag reduction as compared to a conventional flat plate. Results presented in this paper indicate that a transition delay of 20% and a drag reduction of 6% is achievable, thereby demonstrating the veracity of biomimicry as a potential avenue to attain improved aerodynamic performance.

Keywords: Laminar Flow Control, Drag Reduction, Forward Facing Steps, CFD, Shark Skin, Biomimetics.

1. Introduction

Transition delay and drag reduction has been the subject of great intrigue and research over the past century. Reduction in drag improved by leaps and bounds in the 20th century, right since the inception of the first airplane by the Wright Brothers. Conventional drag reduction methods have been investigated in detail and have now reached a stage where any further gains in drag reduction have levelled off. Extensive literature is available on conventional drag reducing mechanisms [1]. To further improve the efficiency of modern aircrafts, as well as reduce noise and emissions, research is now being actively focused on alternate drag reducing mechanisms. One such alternate drag reducing mechanism is presented by the authors in this paper in the form of biomimetically inspired Forward Facing Step (FFS).

The concept of the FFS has been inspired by the texture of the shark-skin. Biomimicry has been proven to provide effective solutions to modern problems in a wide variety of scenarios [2], [3]. Biomimetics in the form of the shark-skin has great potential in developing alternate drag reducing mechanisms [4]. The shark-skin consists of multiple placoid micro scales placed on top of each other in the form of a series of steps along the direction of flow (shown in Fig. 1). These micro scales are of the order of $2 - 3 \mu m$ in height. The FFS is a simplified geometry based on the micro scales placed on top of each other and makes use of a single step instead of a multi-step configuration (that mimics the placoid scales). The use of shark-skin inspired features have shown great promise in drag reduction. The efficacy of shark-skin inspired micro-features has been demonstrated by Bhatia et al. through the use of sinusoidal surface waves on the surface of a flat plate [5]. The use of these surface waves resulted in a transition delay of 10.8% and an overall drag reduction of 5.2%.

The study of geometric features such as steps has been of great interest to aerodynamicists in terms of flow separation and reattachment. However, most of the existing literature focuses extensively on Backward Facing Steps (BFS) geometric configurations to analyse the flow structure behind the step. The BFS cases have been extensively reviewed by several authors [7]–[9]. Flow over a FFS has recently started receiving attention as compared to BFS especially in turbulent boundary layers [10]–[12]. The effects of step height and velocity on the flow topology of an FFS were studied experimentally by Stüer et al. [13] and Largeau and Moriniere [14]. Some of the key characteristics of the flow structure as discovered by the researchers mentioned above were that the presence of the FFS acts as a blockage and results in the formation of an adverse pressure gradient. The presence of this adverse pressure gradient causes flow separation upstream of the step and reattachment downstream of the step [15]. The flow mechanism of the FFS is shown in Fig. 2.



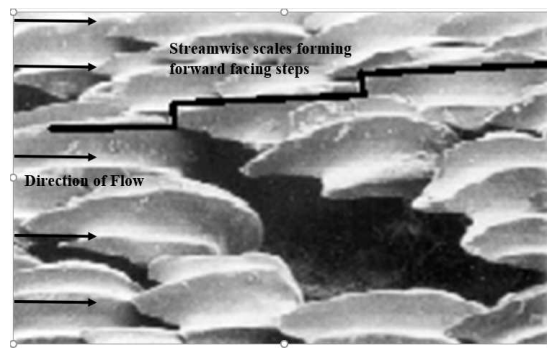


Fig. 1. Placoid scales on the shark-skin forming forward facing steps of $2 - 3\mu\text{m}$ in the streamwise direction. Adapted with permission [6]. Reproduced with permission from *Advanced Functional Materials* 23, 36 (2013). Copyright 2013 John Wiley and Sons

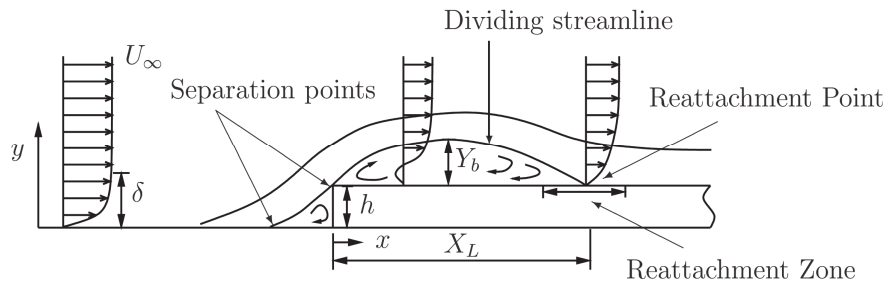


Fig. 2. Flow Mechanism over an FFS depicting separation and reattachment points (Sherry, Lo Jacono, and Sheridan, 2010). Reproduced with permission from *Journal of Wind Engineering and Industrial Aerodynamics* 98, 12 (2010). Copyright 2010 Elsevier

This phenomenon takes place due to the blunt shape of the FFS. Local mixing and turbulent intensity increase within the boundary layer due to the presence of the step. The primary cause for reattachment is turbulent mixing. Separation above the step causes a momentum deficit. The turbulent mixing enables higher velocity free stream fluid to flow into the reattachment zone to overcome this deficit. Several researchers have studied the effects of boundary layer thickness to step height ratio (δ/h) on the recirculation zone. Previously conducted research indicates that the reattachment due to FFS greatly depends on the (δ/h) ratio [17], [18]. When $\delta/h > 1$, the reattachment length greatly depends on the Reynolds number i.e. the velocity [16]. However, when $\delta/h < 1$ the reattachment length is independent of the δ/h ratio. In such cases, Sherry et al. [16] conclude that the reattachment point is usually situated in a range of $4h - 5h$ from the start of the step and greatly depends on the Reynolds number [14], [19]. When $\delta/h \ll 1$, there is direct interaction between the free stream velocity and the FFS. Sherry et al. [16] opine that in this case, as the free stream velocity is larger than the velocity in the boundary layer, interaction between the blunt body and the free stream velocity will cause a significant perturbation of the flow field and will result in the mixing of free stream fluid and boundary layer fluid. The flow structure over the FFS in this case resembles the flow over a blunt plate and there is flow separation without reattachment [16], [20]. Another factor that is of crucial importance to the flow mechanism over an FFS is the model length to height ratio (L/h) as it greatly impacts the flow structure. Previously conducted research indicates that when the $\delta/h < 1$, a minimum L/h ratio of 4 is required to negate the effects of trailing edge separation on the flow structure due to the presence of the FFS [21]. However, when $\delta/h > 1$ the minimum L/h of 1.75 negates the effects of the trailing edge separation [22]. Thus, to focus singularly on the impact of the FFS on the flow structure and to eliminate the effect of the trailing edge separation, the L/h ratio has to be carefully considered.

While much work has been conducted in the study of the recirculation zone and the δ/h ratio, the correlation between the step height and boundary layer transition in subsonic flow has not been documented in detail. The impact of a FFS on boundary layer transition has been analysed experimentally by Wang and Gaster [23]. Results from Wang and Gaster indicate that an increase in the step height from 0.5 mm ($\delta/h \sim 3.8$) to 2 mm ($\delta/h \sim 1.9$) brings transition closer to the step location. An increase in velocity has the same impact and for a given step height, an increase in velocity will result in earlier transition and bring the transition location closer to the step location. Transition onset has also been observed to be earlier as compared to a flat plate with no step. Thus, the use of the FFS in this case has shown to bring transition onset forward and is considered to be a surface imperfection. However, a FFS with a slot in it to re-energise the flow has been patented and demonstrates drag reduction ranging from 2-6% [24].

Most of the literature presented in this section demonstrates the use of FFS that are high enough to perturb the flow significantly. Apart from this, most of the FFS are placed within the turbulent boundary layer. The authors believe that the use of a strategically placed micro FFS of the order of shark-skin scales within the laminar boundary layer can result in transition delay and drag reduction. This forms the fundamental hypothesis of this paper.

2. Methodology

Modelling of the FFS is an extremely vital step to accurately capture the flow phenomenon fore and aft of the step. The presence of the FFS will invariably impact the boundary layer transition onset location as well as the drag.

2.1 Model Setup

A flat plate baseline geometric model is chosen based on existing literature to ensure reliability in CFD modelling is attained [25], [26]. Validation of the authors' results is conducted using well published cases from literature. The flat plate model and the FFS model are shown in **Fig. 3** (a), (b) and **Fig. 4** shows the mesh and the boundary conditions. The computational method, settings and input parameters are given in Table 1.



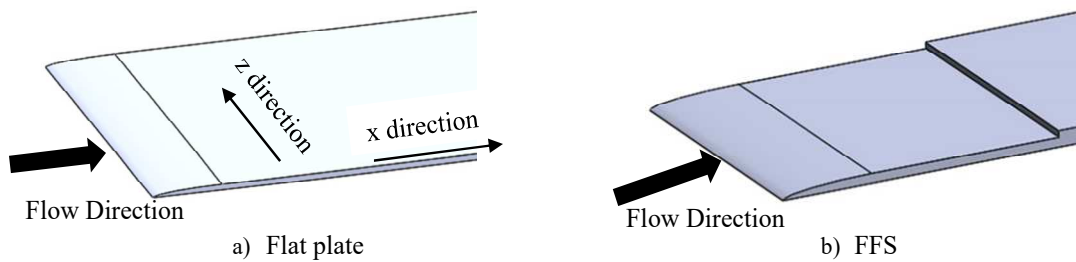


Fig. 3. 3D representation of a) the 2D flat plate, b) 2D plate with FFS. In both cases, flow direction is perpendicular to the leading edge. The x axis is oriented along the streamwise direction whereas the z axis is along the spanwise direction. The y axis is perpendicular to the xz plane.

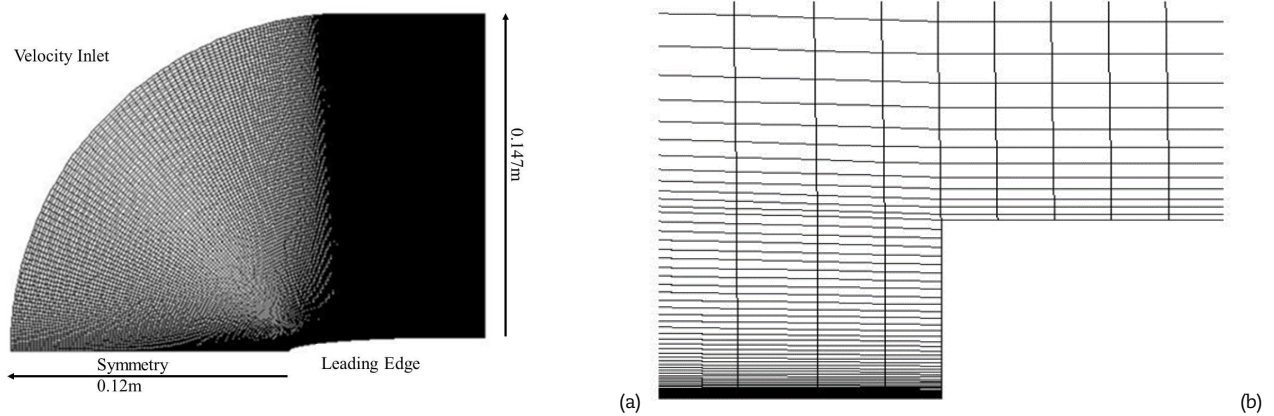


Fig. 4. (a) Mesh with boundary conditions clustered around the leading edge and (b) Magnified view of the mesh around the FFS

A structured multi-block mesh with 400,000 elements is chosen based on grid independence studies. The mesh possesses high density elements clustered around the leading edge as well as the FFS (Fig. 4 (a)). The dimensions of the mesh as well as the boundary conditions are chosen from existing literature [25]. The velocity inlet is placed 0.12m from the leading edge and the domain extends 0.5m behind the plate model. The height of the domain is 0.147m. A no-slip boundary condition is used for the wall along with a velocity inlet and a pressure outlet. All other boundaries are given a symmetry boundary condition. The wall expansion ratio is 1.07 and the y^+ is maintained at 0.1. Mesh elements are also clustered around the FFS to ensure accurate resolution of flow features (shown in Fig. 4 (b)). A minimum first cell height of 0.0009mm was maintained from the step.

All simulations are performed in ANSYS FLUENT. Solver settings are chosen based on existing literature [25], [27]–[30]. The diffusion coefficient $\sigma_{\theta t}$ was changed from its default value of 2 to 10 based on data presented by Lin et al. that demonstrated the suitability of the Transition SST model with a diffusion coefficient of 10 in a number of non-flat geometry scenarios such as surface waves and BFS to accurately predict transition onset. The computational setup has also shown great efficacy in simulating micro-features at a scale similar to the FFS and has accurately depicted the flow structure around these micro-features. As a result, the authors believe that the computational setup is suitable, reliable and can accurately depict the flow features for the FFS presented in this paper.

2.2 Validation and Reliability of Simulations

The Transition SST model is a correlation based model that has been developed from experimental test cases encompassing a wide variety of scenarios [27]. Transition onset locations for the Transition SST model have been found to be accurate for flat plates as well as aerofoils.

For the purpose of validation, initially, the Transition SST model is used to benchmark classical cases from different authors to set up a baseline for further simulations [25], [30]. Benchmark results presented in Fig. 5 (a) shows good correlation to the experimental transition onset location of the Schubauer Klebanoff TSK experiment [26] as well as the simulated transition onset location presented by Lin et al. (2012). Transition onset for Menter’s simulation is roughly 14% earlier as compared to the TSK experiment.

Table 1. Geometry, model, and detailed computational setup

Geometry	Flat plate with quarter elliptical leading edge of aspect ratio 12
Plate size	Length: 1.8m , Thickness: 0.006m
Grid	Structured Multi-Block 400,000 elements
CFD Model	Transition SST with diffusion coefficient $\sigma_{\theta t}$
Solver	Steady State pressure based
Scheme	Second Order SIMPLE for pressure, momentum, and turbulence. Least Square Cell Based discretization for the gradient
Input parameters	Velocity: 50ms ⁻¹ ,Turbulence Intensity (Tu): 0.18% and Kinematic Viscosity (ν): 1.46 × 10 ⁻⁵ m ² s ⁻¹



Table 2. Reattachment length comparison for authors vs. Sherry et al. [16]

Study	δ / h	Re_h	x / h
Sherry et al.	1.25	6.66×10^3	3.4
Authors	1.25	6.66×10^3	3.6

The simulations are then validated against standard FFS experimental test cases presented in (Sherry et al., 2010; Wang and Gaster, 2005). The key parameter to be tested in the case of an accurate FFS simulation is the length of the reattachment zone downstream of the step (Table 2) as well as the transition onset location due to the presence of the FFS (Fig. 5 (b)).

A comparison of the reattachment length for the authors vs. existing literature (Table 2) indicates that the simulation method and the model chosen by the authors accurately captures the length of the reattachment zone. The reattachment zone for the authors is roughly 5% longer than for Sherry et al. Validation of the transition onset location is conducted by using a normalised plot of the Mach number (M) against the distance from the leading edge (x/L). The normalised transition onset location when compared to Wang and Gaster demonstrates accurate transition onset for a 0.5 and 2.0 mm step heights at different velocities. However, transition onset locations presented by the author, at 1 mm step height, indicate that simulations over-predict the transition onset location albeit with a very similar trend to experimental data (Fig. 5(b)). Transition onset, in this case, is later and within a range of 6-15%.

In the presented validation cases, the authors simulated results deviate from the reattachment length as well as with the experimental transition onset values provided by Wang and Gaster. These deviations can be attributed to the fact that no data has been provided for uncertainty analysis carried out for experimental results and it is widely accepted that most experimental results are subject to human and equipment error. Wang and Gaster, in their paper, have also highlighted that variations in the measured transition onset locations are mainly due to the different methods used to determine the inception point of transition as well as due to the variation in the levels of turbulence intensity that exists in the different wind tunnels. As a result, simulated results can vary from experimental results in certain cases but can accurately depict the trend of the transition onset location. Thus, it can be concluded that results presented for the flat plate as well as the FFS indicate reliability, repeatability as well as accurate capture of the flow phenomenon by the authors simulations methods.

3. Results

In this section, results are presented in the following order: Section 3.1 provides a case study of the flow over the FFS and its comparison to the flat plate. The flow phenomenon over the FFS is explained using classical plots such as the velocity profile, the pressure coefficient C_p and the skin friction C_f . Velocity and the Turbulent Kinetic Energy (TKE) contours are used to highlight the flow structure of the boundary layer. The potential mechanism of transition delayed by FFS is proposed. Section 3.2 provides the impacts of a strategically placed FFS within the laminar boundary layer. The step height is changed to control flow separation due to the FFS and to attain transition delay and drag reduction. Finally, Section 0 depicts the influence of a change in the velocity on boundary layer transition and drag reduction.

3.1 Boundary Layer Flow on FFS vs. Flat Plate

A comparative analysis of the FFS versus the flat plate is provided in this section. Boundary layer flow development is analysed for a FFS placed at $x/L = 0.4$ with step height of $\delta/h = 24.4$ at the given velocity of 50.1ms^{-1} .

The normalised velocity contour (Fig. 6 (b)) of the FFS is placed alongside a similarly scaled plot of the flat plate (Fig. 6 (a)). The velocity contour is plotted with the local Reynolds number (Re) on the X axis and the normalised height y/Y along the Y axis. The key differences in the velocity distribution are observed at the edge of the low velocity region/layer (defined as the velocity layer up to $u/U = 0.3$) as well as the edge of the boundary layer (encircled). The FFS results in an obvious pushing up of the low velocity region as well as a very mild pushing up of the boundary layer at its edge.

A comparison of the turbulent kinetic energy (TKE) highlights the differences in the growth of the disturbance within the boundary layer for the FFS (b) vs. the flat plate (a) (Fig. 7). The turbulent boundary layer is characterised by high TKE values. The red region $\geq 3 \text{m}^2 \text{s}^{-2}$ in the contour plot depicts the setting in of high turbulence and is a precursor to the onset of the turbulent boundary layer. The start of the red region of the FFS shows a delay for FFS in the TKE when compared to the flat plate. It can be observed that for the flat plate, the red region in TKE plot starts at about $Re_x = 2.62 \times 10^6$ as opposed to $Re_x = 2.72 \times 10^6$ for the FFS. In addition, when this red region has approached the surface of the plate, transition onset is observed. The delay of transition onset for FFS as compared to flat plate is shown in Fig. 8.

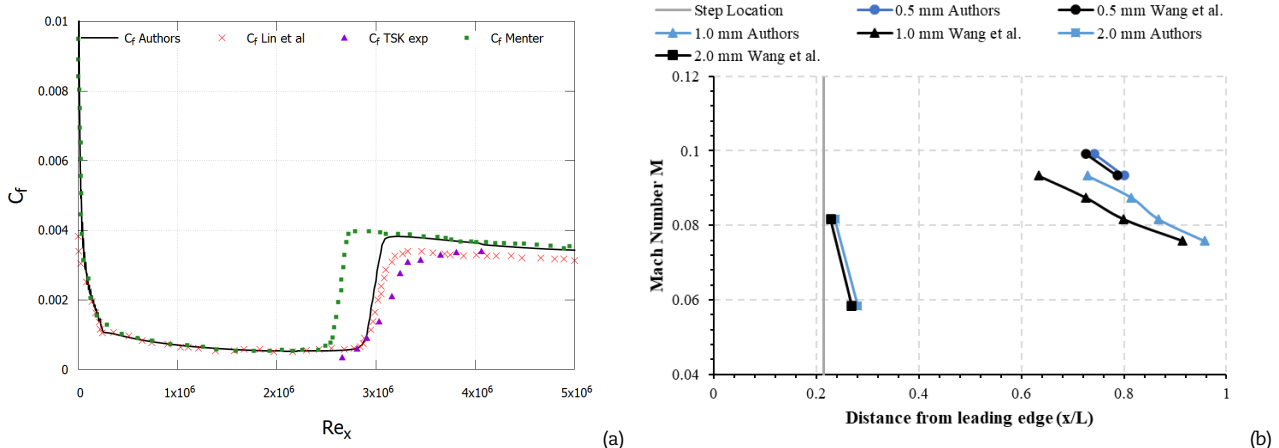


Fig. 5. (a) Flat Plate Benchmarking and model validation against existing experimental and simulation cases
(b) Validation of transition onset locations at different step heights and free-stream velocities compared with Wang and Gaster [23]



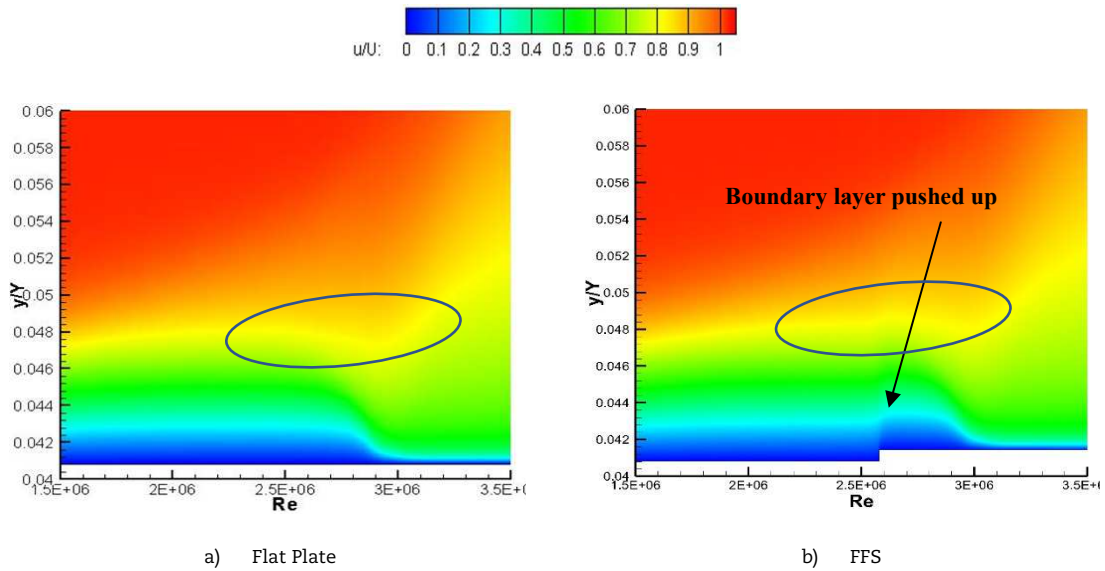


Fig. 6. Normalised Velocity Contours for the Flat Plate (a) and the FFS (b). Contours are plotted with the Local Reynolds number on the X axis and the normalised height on the Y axis.

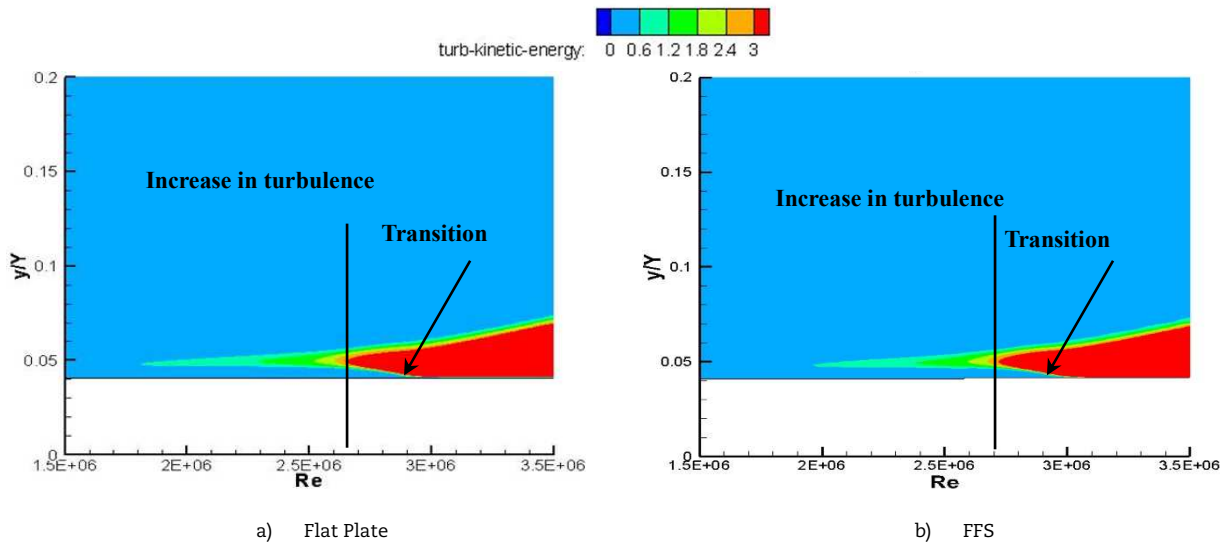


Fig. 7. TKE Contours for the Flat Plate (a) and the FFS (b). Onset of disturbance within the boundary layer is highlighted for both cases

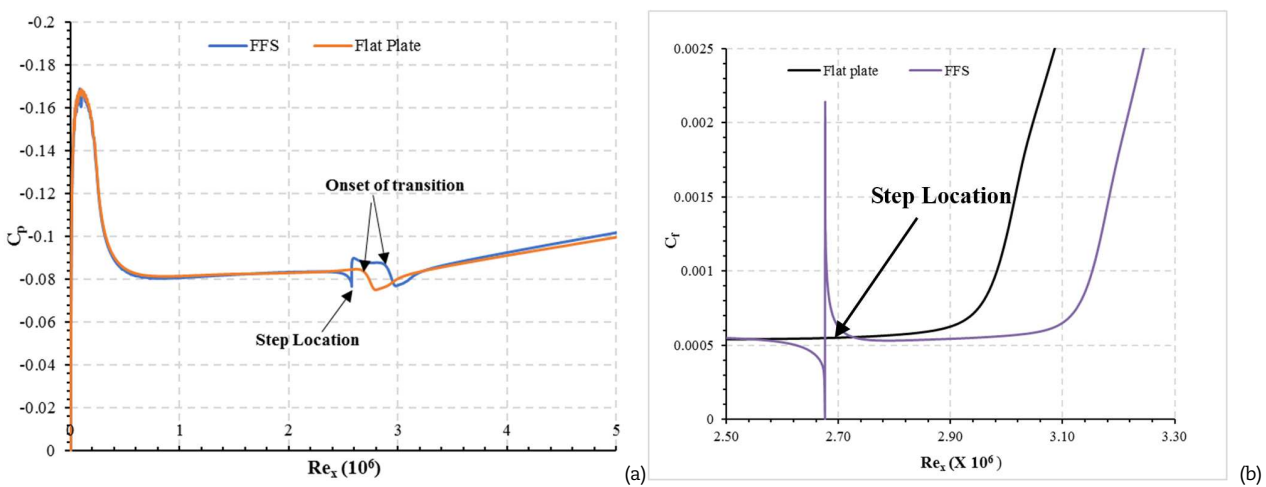


Fig. 8. (a) Pressure coefficient for the FFS and the flat plate plotted against the local Reynolds number. (b) Skin friction coefficient (C_f) plotted against the local Reynolds Number (Re_x) for the FFS and the flat plate. The FFS depicts a sharp drop and rise in the skin friction at the step location as indicated



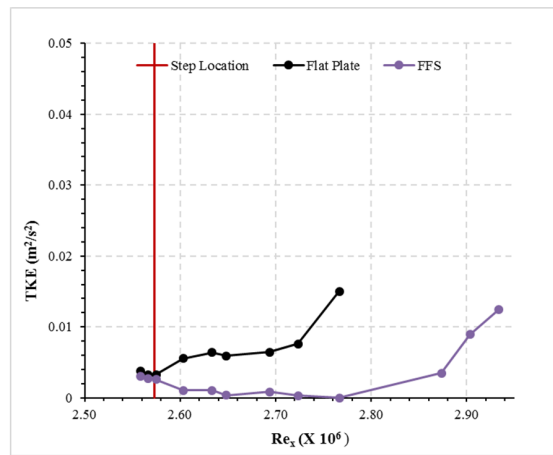


Fig. 9. TKE development over the flat plate and the FFS. The step location is shown in red and is indicative of the position only

The plot for the pressure coefficient C_p also demonstrates the impact of the FFS in resulting in a more negative pressure difference on the top surface of the plate (**Fig. 8 (a)**). When the fluid first encounters the FFS, the pressure increases (along the vertical wall of the step) due to the profile of the step. On top of the step, the pressure reduces resulting in a more favourable pressure distribution. Behind the FFS, the region of favourable pressure gradient extends until transition onset takes place. After the region of favourable pressure gradient, the impact of the step on the pressure can be visibly observed and the sharp kink after the step denotes the onset of transition. The presence of the FFS clear demonstrates a delay in transition onset.

A comparison of the skin friction coefficient (**Fig. 8 (b)**) suggests that the presence of the FFS results in a region of varied skin friction ranging from near zero at bottom of the step to a value of 0.0021 at the top of the step. Therefore, the skin friction depicts the obvious disturbances introduced to the system by FFS. Further analysis of the local skin friction should lead to identify some of the primary reasons of transition delay.

The skin friction visibly reduces aft of the step as compared to the flat plate. The calculated skin friction coefficients indicate that from the position of the step to the transition onset, the skin friction coefficient for FFS is on an average 8.4% lower than that for the flat plate, despite the sharp rise in skin friction at the location of the step. This net deficit in skin friction is one of the primary reasons for transition delay. Transition is delayed by 6.1%.

The development of the TKE over the plate and the FFS demonstrates the differences between the flow development over the plate and the FFS (**Fig. 9**). The development of the TKE over the flat plate and the FFS indicates that initially before the step, the flat plate and the FFS have near identical TKE values and follow a very similar trend. The difference between the flat plate and the FFS is visible in the region aft of the step. The trend for the flat plate indicates an increase in the TKE whereas the TKE decreases for the FFS after the step. At about $Re_x = 2.6 \times 10^6$, the TKE for the FFS is 81% lower than the flat plate. Also, it is observed that the TKE for the flat plate shows a sharp increase in the value at about $Re_x = 2.73 \times 10^6$ whereas the TKE for the FFS shows this increase at about $Re_x = 2.88 \times 10^6$ and returns to a similar trend to that of the flat plate. The TKE is an indicator of the disturbance and its amplification within the boundary layer. Therefore, the trend from **Fig. 9** indicates that the presence of the step damps the disturbance within the boundary layer as opposed to the flat plate. This is one of the other primary reasons for the transition delay. These damping effects can also be correlated to the fact that the presence of the FFS results in a favourable pressure gradient, thereby preventing the amplification of disturbances within the boundary layer.

This deficit in skin friction and transition delay influences the drag as well. The computed C_d values indicate that drag in the laminar region is 2.9% lower than the flat plate. The total drag over the length of the FFS surface is 0.39% lower than the total drag for the flat plate. Thus, results in this section indicate that the presence of the step reduces the regional skin friction and damps the disturbance which delays transition and reduces drag.

3.2 Impact of Step Height on Boundary Layer Transition

Results presented in this section demonstrate the impacts of changes in the height of the FFS on boundary layer transition and the drag. The test cases are allocated based on the normalised location of the step (x/L) in the laminar boundary layer. The step heights are varied based on the (δ/h) ratio. The boundary layer thickness δ is computed from the laminar boundary layer thickness of the flat plate at each (x/L) location and at a velocity of 50ms^{-1} .

At each step location, the step heights are changed until the detrimental impact of the step is reduced. Some test cases demonstrate flow separation. Step heights in the test cases are smaller than the low velocity layer near the plate surface ($u/U < 0.3$). Selective test cases are enlisted in Table 4.

3.2.1 $x/L = 0.1$

When the step is placed at $x/L = 0.1$, all three step heights have a detrimental impact on transition onset (**Fig. 10**). All three steps are characterised by a sharp jump in the wall shear stress at the step location. The presence of the largest step height ratio (lowest step height) results in earliest transition onset. Step height ratio of 12.2 has the least impact on transition onset.

The computed transition onset and drag values indicate that transition is about 6% earlier for step height ratio of 48.8 and sequentially reduces to about 3.2% for a step height ratio of 12.2. Drag is higher than the flat plate by a maximum of about 6.6% for the step height ratio of 48.8

Table 3. Boundary layer thickness δ at different (x/L) locations

x/L	Boundary layer thickness δ (m)
0.1	0.0006
0.2	0.00112
0.4	0.0022



Table 4. Allocation of FFS test cases based on changes in the (δ / h) ratio at different x / L

Step location (x / L)	Step height (δ / h)		
0.1			
0.2	48.8	24.4	12.2
0.4			

Table 5. Transition delay and computed drag values for different step height ratios at $x / L = 0.1$

δ / h	Transition Delay (%)	Drag Reduction %
0	0	0
48.8	-6.18	-6.66
24.4	-4.67	-3.22
12.2	-3.22	-3.70

Table 6. Transition delay and computed drag values for different step height ratios at $x / L = 0.2$

δ / h	Transition Delay (%)	Drag Reduction %
0	0	0
48.8	-3.66	-0.21
24.4	-5.53	-0.73
12.2	-6.56	-1.78

Thus, contrary to the perception that a larger step height will result in the earliest transition onset, at $x / L = 0.1$, the presence of a larger step height has the least impact on the transition onset location even though, the performance is worse than the flat plate. The drag for $\delta / h = 24.4$ is the least amongst the three step height ratios. All three FFS show higher drag than the flat plate.

The development of the TKE due to the presence of the step provides crucial information to the growth of disturbance within the boundary layer (Fig. 11). The development of the TKE is presented at selective locations from 5% before the step to selective locations after the step showing sharp changes in the TKE (Fig. 11 (a), (b)). TKE results from (a) indicate that in the region just preceding the step, the TKE for the step is higher than that of the flat plate by about 11%. The presence of the step causes a drastic increase in the TKE. The magnitude of the TKE is 40% higher than that of the flat plate at the step location. Just after the step, the TKE value drops sharply. At about $Re_x = 0.6 \times 10^6$, the TKE value for the step is 7% higher than the flat plate. Thereafter, the FFS and the flat plate show a similar trend with the FFS consistently demonstrating higher TKE. At about $Re_x = 2.3 \times 10^6$, the FFS shows a sharp increase in the TKE. This sharp increase in TKE is a possible indicator of the rapid growth of disturbance within the boundary layer. Rapid increase in the TKE is suggestive of early transition onset.

Thus at $x / L = 0.1$, the presence of the FFS is a source of disturbance. The FFS demonstrates increased TKE activity due to the step and the TKE is consistently higher than the flat plate. Thus, the presence of a FFS results in a net increase in the TKE thereby strongly indicating an increase in the growth of disturbance within the boundary layer leading to early transition onset and increased drag.

3.2.2 $x / L = 0.2$

The presence of the step at $x / L = 0.1$ presented in the preceding subsection demonstrates early transition onset. Therefore, the authors decided to move the step further downstream in the laminar region at $x / L = 0.2$. Results are plotted for three key step height ratios viz. $\delta / h = 48.8, 24.4, 12.2$.

The skin friction C_f plotted for different step height ratios indicates that the presence of step at $x / L = 0.2$ causes early transition onset for all step height ratios. The computed transition delay and drag values are presented in Table 6.

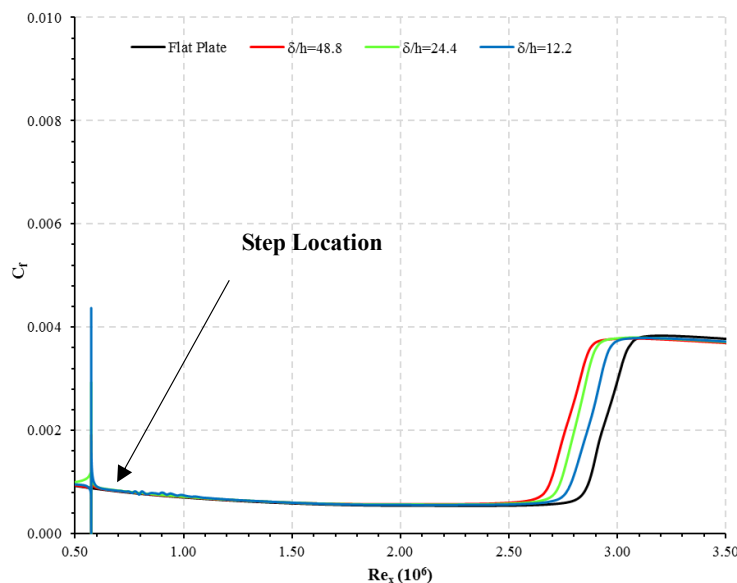


Fig. 10. Skin friction coefficients for $\delta / h = 48.8, 24.4, 12.2$ at $x / L = 0.1$



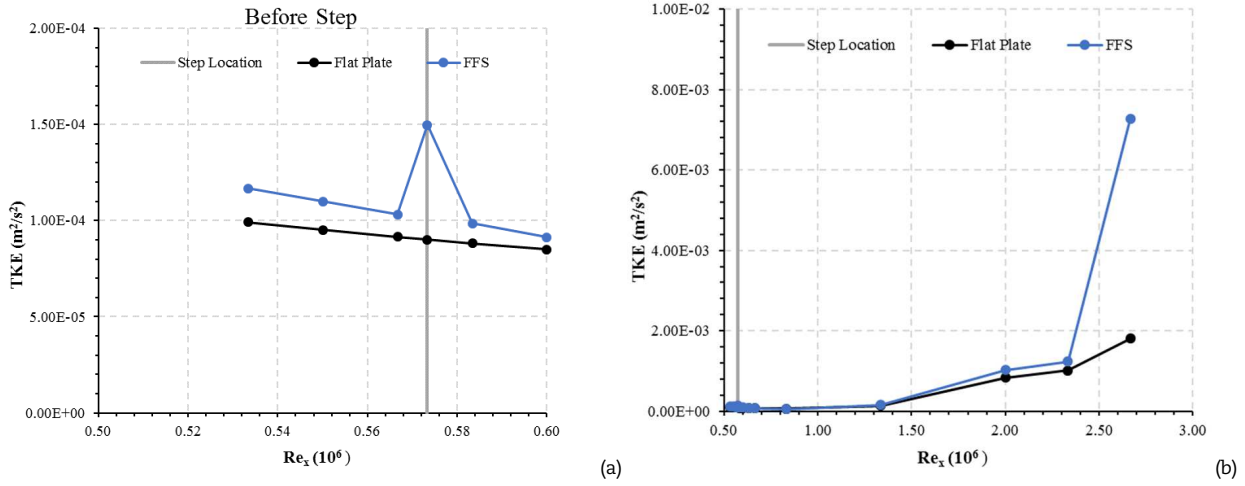


Fig. 11. Development of TKE on and after the step at $x / L = 0.1$

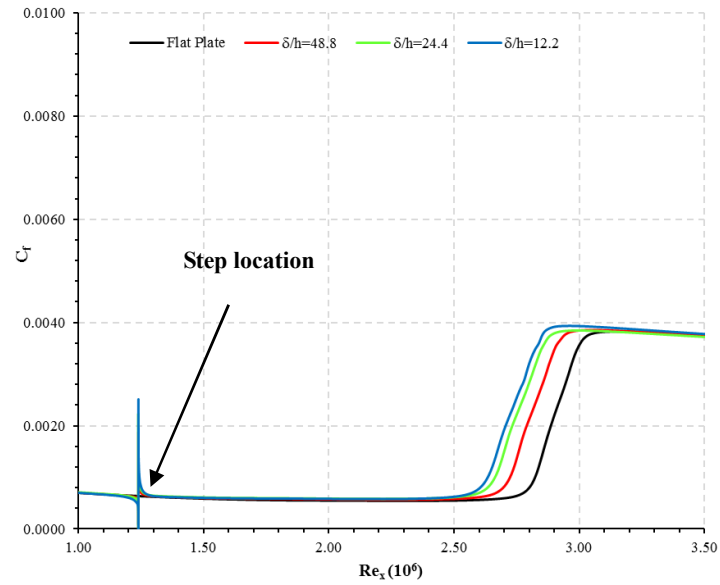


Fig. 12. Skin friction coefficients for $\delta / h = 48.8, 24.4, 12.2$. Transition delay is observed at $\delta / h = 24.4$

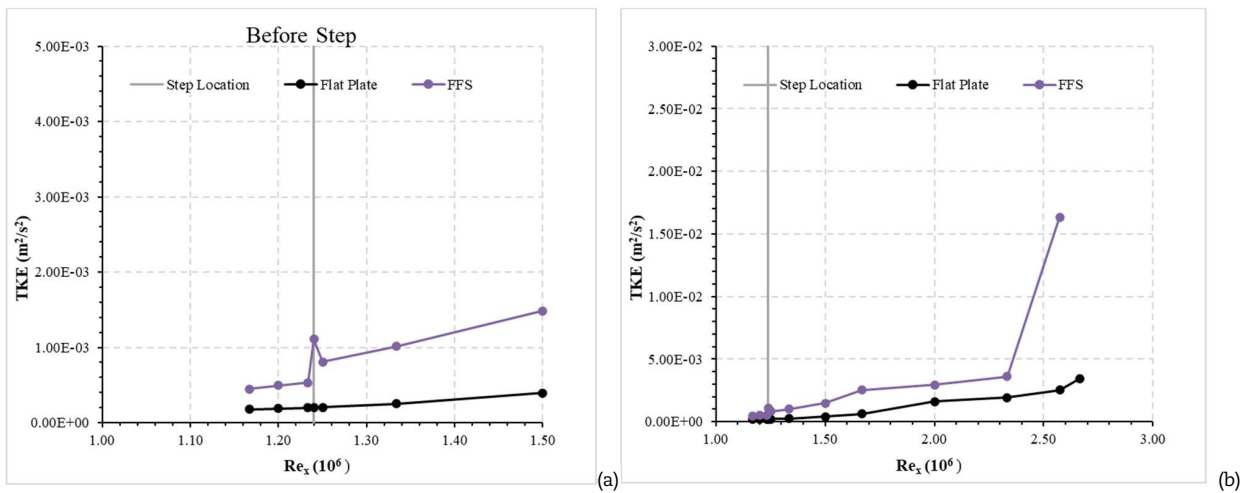


Fig. 13. Development of TKE on and after the step at $x / L = 0.2$



Table 7. Transition delay and computed drag values for different step height ratios at $x/L = 0.4$

δ/h	Transition Delay (%)	Drag Reduction %
0	0	0
48.8	5.53	1.45
24.4	4.52	0.61
12.2	-3.22	-3.46

The computed transition onset and drag values indicate that at $x/L = 0.2$, transition onset and the drag do follow a reversed sequence as compared to $x/L = 0.1$. Thus, at $x/L = 0.2$, as the step height ratio increases, the impact of the FFS on the boundary layer flow diminishes. At $\delta/h = 48.8$ the drag is 0.2% higher than the flat plate. The change in location of the step from $x/L = 0.1$ to $x/L = 0.2$ plays a critical role in defining the flow structure around the FFS as well as the boundary layer flow. Drag values at $x/L = 0.2$ are at least half of those at $x/L = 0.1$.

Like $x/L = 0.1$, the TKE development before and after the step is compared to the flat plate (**Fig. 13** (a),(b)). The presence of the step causes an increase in the TKE in the region 5% before the step. The TKE on an average is 60% higher than that for the flat plate. At the top of the step, the TKE shows a jump. The TKE at this location is 82% higher than the flat plate. After the step, the TKE drops sharply. At this point, the TKE is about 74% higher than the flat plate.

Thereafter, the TKE shows a similar trend to the flat plate (**Fig. 13** (b)). At about $Re_x = 2.3 \times 10^6$, the TKE for the FFS rises sharply. Like $x/L = 0.1$, this sharp increase in the TKE indicates that the disturbance within the boundary layer has grown which results in early transition onset.

Thus, the presence of the FFS further along the plate has a lower detrimental impact on the boundary layer.

3.2.3 $x/L = 0.4$

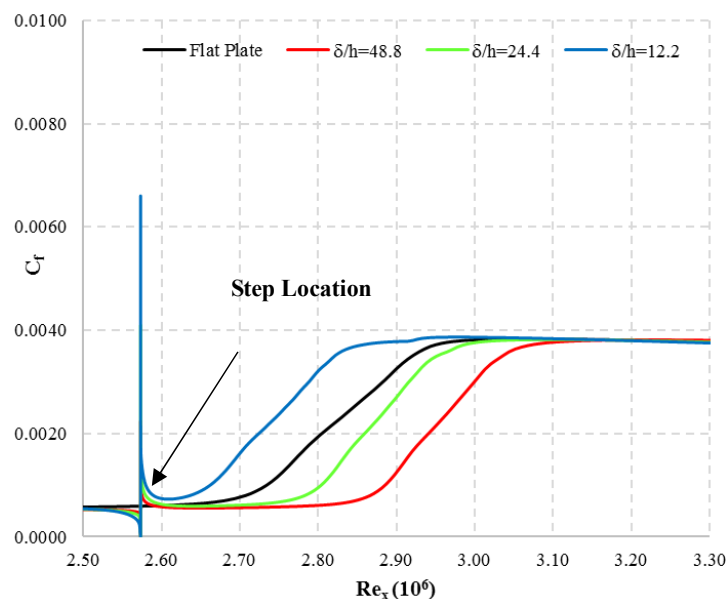
As the step at $x/L = 0.2$ led to an increase in drag and earlier onset of transition, the step was moved further downstream to $x/L = 0.4$. In the absence of a step, boundary layer transition occurs at $x/L = 0.47$. The step in this case is placed very close to original transition onset location. The step is located strategically at 10% before the flat plate transition onset location. Once again, the three step height ratios of $\delta/h = 48.8, 24.4, 12.2$ are considered.

The skin friction coefficient C_f for each step height ratio demonstrates that the presence of the step just before the transition region leads to a delay in transition (**Fig. 14**). Transition delay increases with an increase in step height ratio. When $\delta/h = 12.2$, transition onset is earlier as compared to the flat plate. Transition delay is observed when $\delta/h \geq 24.4$ (**Fig. 14**).

It is evident from **Fig. 14** that the impact of the step is greatly governed by the step height ratio. Smaller the step height ratio, larger is the peak skin friction of the step. For $\delta/h = 12.2$, the presence of the step causes a sharp increase in the skin friction at the step. After the step, the skin friction does not recover to the same value as that of the flat plate and remains consistently higher. Thus, the presence of a large step height (and low step height ratio) causes sharp increase in the skin friction thereby promoting early transition onset as compared to the flat plate. In the case of $\delta/h = 24.4$, the skin friction drops after the step and is 15% lower than the step on an average. For $\delta/h = 48.8$, this deficit in skin friction is 20% on an average. The presence of a deficit in the skin friction and therefore the wall shear stress is a crucial indicator of the positive impact of the step on the flow.

The development of the TKE on the FFS and the flow structure has been described in detail in Section 3.1 and highlights the fact that the TKE for the FFS is consistently lower than the flat plate depicting a slower growth rate of the disturbance within the boundary layer (**Fig. 9**).

The computed transition and drag values indicate that a maximum transition delay of 5.53% is attainable at $\delta/h = 48.8$ and the corresponding drag reduction is 1.45% (Table 7).

**Fig. 14.** Skin friction coefficients for $\delta/h = 48.8, 24.4, 12.2$ at $x/L = 0.4$ 

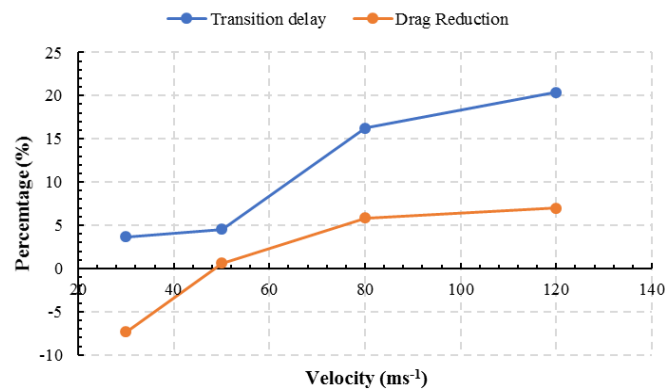


Fig. 15. Transition delay and drag reduction for FFS at different velocities

3.2.4 Impact of Velocity

The presence of the FFS at $x/L = 0.4$ presented in the preceding section shows transition delay and drag reduction. Results presented earlier are all obtained at a velocity of 50.1ms^{-1} . The FFS is also tested for different incoming flow velocities to gauge its suitability with a change in the incoming flow velocity. Thus, the FFS with $\delta/h = 24.4$ is tested at $30, 50.1, 80$ and 120ms^{-1} , respectively. The rationale behind using $\delta/h = 24.4$ is that it is the lowest step height ratio (and consequently the largest step height) that depicts transition delay and drag reduction. The step locations were modified to ensure that for each change in the velocity, the steps are located 10% before the flat plate transition onset location.

The computed transition delay and drag reduction values for the FFS at different velocities (Fig. 15) indicate that the transition onset is delayed and drag reduces as the velocity is increased. At 30ms^{-1} , although transition delay is observed, drag is still considerably higher as compared to the flat plate. Slight drag reduction is observed at 50.1ms^{-1} . The transition delay and drag show a marked increase above 50.1ms^{-1} . A 20% transition delay and a 6% reduction in drag is observed at 120ms^{-1} . Thus, it can be observed that transition delay and drag reduction markedly improves with an increase in velocity.

4. Discussions

Results for the impact of the FFS on boundary layer transition and drag reduction are presented in subsections 3.1, 3.2 and 0. Analysis of the flow structure over the FFS is compared to a standard flat plate in subsection 3.1. The presence of the FFS within the low velocity layer causes a pushing up of this layer as opposed to the flat plate (Fig. 6). The pushing up of the low velocity layer as well as the computations for the TKE indicates that the step has a positive impact on transition delay. The coefficient of pressure (C_p) comparison between the flat plate and the FFS (Fig. 8) indicate that the presence of the FFS results in a favourable pressure gradient aft of the step. This is also corroborated by the TKE comparison between the flat plate and the FFS (Fig. 9). The TKE values for the flat plate and the FFS are nearly identical before the step but are appreciably lower for the FFS than the flat plate. The authors believe that the presence of the FFS plays a key role in damping the disturbances within the boundary layer. The pushing up of the low velocity layer as well as the boundary layer edge results in a favourable pressure gradient. The presence of the favourable pressure gradient might result in mixing of faster moving freestream air with the air within the boundary layer thereby “energising” the boundary layer. This ‘damping’ and ‘energisation’ has an impact on the transition onset and the drag values. Drag in the laminar region is 2.9% lower whereas the overall drag is 0.39% lower. The presence of the strategically placed FFS in the laminar region is one of the primary reasons for the reduction in drag in the laminar region. Thus, in contrast to existing literature, the FFS in this case can no longer be considered to be a surface imperfection.

In subsection 3.2, the location of the step within the laminar boundary layer is varied. When the step is placed near the start of the flat plate ($x/L = 0.1$), the presence of the step causes early transition onset and increased drag. Transition is 3.2% earlier and drag is 3.6% higher than the flat plate in the best possible case that is simulated. When the step is moved further along the plate ($x/L = 0.2$), the FFS shows improved drag values and are closer to the flat plate as compared to when the FFS was at $x/L = 0.1$. Transition onset in the best possible case is 3.6% earlier than the flat plate whereas drag is 0.2% higher than the flat plate. At both $x/L = 0.1$ and $x/L = 0.2$, the presence of the step causes a sharp rise in the TKE at the step location (Fig. 10 and Fig. 12). The TKE is consistently higher than the flat plate after the step. Thus, the presence of the FFS at these locations provides an impetus to the amplification of disturbances within the laminar boundary layer resulting in early transition onset and increased drag.

When the step is moved to $x/L = 0.4$ (10% before the transition onset point for the flat plate), simulations conducted by the authors depict transition delay and drag reduction for $\delta/h \geq 24.4$, whereas only $\delta/h = 12.2$ shows earlier transition onset and higher drag than the flat plate. The steps in the case of $\delta/h \geq 24.4$ are smaller than a quarter of the thickness of the low velocity layer. Thus, the lower the step is within the low velocity layer, the more positive its impact on the boundary layer. The FFS act as micro-features on the surface of the flat plate in a similar manner to the surface waves simulated by Bhatia et al [5]. Both the FFS and the surface waves are manifestations of the micro-features found on the surface of the shark-skin. It can be concluded that drag reduction greatly depends on the step height and the velocity in a manner similar to the live shark skin which tends to adapt its micro-features to its surroundings. The live shark skin changes the parameters of its micro-features such as the height and orientation based on incoming flow conditions to ensure minimal drag.

The impact of the velocity on FFS is described in subsection 0. The impact of the FFS on transition onset and drag reduction is greatly determined by the incoming flow velocity. As the velocity of the incoming flow increases, the effectiveness of the FFS increases (Fig. 15). At the lowest velocity of 30ms^{-1} , the presence of the FFS causes increased drag even though transition delay is observed. Drag values are better than the flat plate from 50.1ms^{-1} onwards. An average commercial aircraft takes off and lands within the range of $50 - 80\text{ms}^{-1}$ [31]. The FFS shows improved flow characteristics and lower drag within the same precise range thereby highlighting the effectiveness of the FFS for take-off and landing scenarios.



5. Conclusions

In this paper, the authors conducted simulations to attain transition delay and drag reduction using a simple and strategically placed FFS within the laminar boundary layer. Based on the results presented by the authors, the following conclusions can be drawn:

1. The presence of the FFS very early within the laminar boundary layer has a detrimental effect on the flow structure.
2. When the FFS is placed 10% before the normal transition onset of the flat plate, transition delay is observed. The critical step height to attain transition delay and drag reduction is $\delta/h \sim 24$.
3. The presence of the FFS results in a favourable pressure gradient aft of the step and leads to a damping of disturbances within the boundary layer. This leads to transition delay and drag reduction.
4. The impact of the FFS increases with an increase in velocity. The FFS shows great practical applications within the range from $50 - 80 \text{ms}^{-1}$.
5. The authors believe that, as the shape of the FFS has not been optimised, a study to identify an optimised step design closely mimicking the shark-skin placoid scales would result in a greater transition delay and drag reduction.

Author Contributions

D. Bhatia developed the hypothesis, undertook a literature review of the concept, performed the CFD simulations and provided the initial analysis for the manuscript; G. Li undertook the mesh independence studies and assessed the CFD modelling; J. Sun performed CFD simulations in conjunction with D. Bhatia and G. Li, and undertook the post-processing tasks. J. Wang proposed the initial concept, provided technical inputs and supervised the project. The manuscript was written through the contribution of all authors. All authors discussed the results, reviewed, and approved the final version of the manuscript.

Acknowledgments

The authors wish to thank the Ningbo Science and Technology Bureau for their funding under the Ningbo Natural Science Programme Project having project code: 2019A610116 as well as the University of Nottingham Ningbo China for their funding under the Faculty of Science and Engineering's New Researcher Grant (NRG). The authors would also like to thank the University of Nottingham Ningbo China and Kingston University London for providing facilities and encouragement to perform the CFD simulations.

Conflict of Interest

The authors declared no potential conflicts of interest with respect to the research, authorship, and publication of this article.

Funding

The authors received financial support for the research, authorship, and publication of this article from the Ningbo S&T Bureau Ningbo under the Natural Science Programme with project code: 2019A610116 as well as the University of Nottingham Ningbo China for their funding under the Faculty of Science and Engineering's New Researcher Grant (NRG).

Nomenclature

BFS	Backward Facing Step	Re_h	Reynolds number based on the height of the step
CFD	Computational Fluid Dynamics	Re_x	Local Reynolds number
C_f	Skin friction coefficient	TKE	Turbulent Kinetic Energy [m^2s^{-2}]
C_p	Pressure coefficient	x	Local length from the leading edge of the model [m]
FFS	Forward Facing Step	x/L	Ratio of local length to the total length of the model
h	Height of the step [m]	δ	Boundary layer thickness [m]
L	Total length of the model [m]	δ/h	Boundary layer thickness to step height ratio
L/h	Model to step height ratio	ν	Kinematic Viscosity [m^2s^{-1}]


References


- [1] D. M. Bushnell, "Aircraft drag reduction—a review," *Proc. Inst. Mech. Eng. Part G J. Aerosp. Eng.*, 217(1), pp. 1–18, 2003.
- [2] P. Ball, "Life's lessons in design," *Nature*, 409, pp. 413–416, 2001.
- [3] R. Cahn, "Learning from nature," *Nature*, 444(7118), pp. 425–425, 2006.
- [4] D. Bhatia and J. Wang, "Biomimetics - A Potential Solution to Drag Reduction in Modern Aerodynamics," *Glob. J. Eng. Sci.*, 3(4), pp. 1-2, 2019.
- [5] D. Bhatia et al., "Transition Delay and Drag Reduction using Biomimetically Inspired Surface Waves," *J. Appl. Fluid Mech.*, 13(4), pp. 1207–1222, 2020.
- [6] G. D. Bixler and B. Bhushan, "Fluid drag reduction with shark-skin riblet inspired microstructured surfaces," *Adv. Funct. Mater.*, 23(36), pp. 4507–4528, 2013.
- [7] J. K. Eaton and J. P. Johnston, "A Review of Research on Subsonic Turbulent Flow Reattachment," *AIAA J.*, 19(9), pp. 1093–1100, 1981.
- [8] L. Chen, K. Asai, T. Nonomura, G. Xi, and T. Liu, "A review of Backward-Facing Step (BFS) flow mechanisms, heat transfer and control," *Thermal Science and Engineering Progress*, 6, pp. 194–216, 2018.
- [9] E. Montazer, H. Yarmand, E. Salami, M. R. Muhamad, S. N. Kazi, and A. Badarudin, "A brief review study of flow phenomena over a backward-facing step and its optimization," *Renewable and Sustainable Energy Reviews*, 82, pp. 994–1005, 2018.
- [10] A. S. Kherbeet et al., "Heat transfer and fluid flow over microscale backward and forward facing step: A review," *International Communications in Heat and Mass Transfer*, 76, pp. 237–244, 2016.
- [11] Y. XUE, J. REN, J. LUO, and S. FU, "Drag increment induced by a small-scale forward-facing step in Mach number 5 turbulent boundary layer flows," *Chinese J. Aeronaut.*, 33(10), pp. 2491–2498, 2020.
- [12] C. A. Edelmann and U. Rist, "Impact of forward-facing steps on laminar-turbulent transition in transonic flows," *AIAA J.*, 53(9), pp. 2504–2511, 2015.
- [13] H. Stüer, A. Gyr, and W. Kinzelbach, "Laminar separation on a forward facing step," *Eur. J. Mech. - B/Fluids*, 18(4), pp. 675–692, 1999.
- [14] J. F. Largeau and V. Moriniere, "Wall pressure fluctuations and topology in separated flows over a forward-facing step," *Exp. Fluids*, 42(1), pp. 21–40, 2006.
- [15] D. Leclercq, M. Jacob, A. Louisot, and C. Talotte, "Forward-backward facing step pair - Aerodynamic flow, wall pressure and acoustic characterisation," in *7th AIAA/CEAS Aeroacoustics Conference and Exhibit*, 2001.



- [16] M. Sherry, D. Lo Jacono, and J. Sheridan, "An experimental investigation of the recirculation zone formed downstream of a forward facing step," *J. Wind Eng. Ind. Aerodyn.*, 98(12), pp. 888–894, 2010.
- [17] M. Agelinchaab and M. F. Tachie, "PIV Study of Separated and Reattached Open Channel Flow Over Surface Mounted Blocks," *J. Fluids Eng.*, 130(6), p. 061206, 2008.
- [18] R. Camussi, M. Felli, F. Pereira, G. Aloisio, and A. Di Marco, "Statistical properties of wall pressure fluctuations over a forward-facing step," *Phys. Fluids*, 20(7), p. 075113, 2008.
- [19] H. Hattori and Y. Nagano, "Investigation of turbulent boundary layer over forward-facing step via direct numerical simulation," *Int. J. Heat Fluid Flow*, 31(3), pp. 284–294, 2010.
- [20] R. Hillier and N. J. J. Cherry, "The effects of stream turbulence on separation bubbles," *J. Wind Eng. Ind. Aerodyn.*, 8(1–2), pp. 49–58, 1981.
- [21] G. Bergeles and N. Athanassiadis, "The flow past a surface-mounted obstacle," *J. Fluid Eng.*, 105, pp. 461–463, 1983.
- [22] I. P. P. Castro and M. Dianat, "Surface flow patterns on rectangular bodies in thick boundary layers," *J. Wind Eng. Ind. Aerodyn.*, 11(1–3), pp. 107–119, 1983.
- [23] Y. X. Wang and M. Gaster, "Effect of surface steps on boundary layer transition," *Exp. Fluids*, 39(4), pp. 679–686, 2005.
- [24] M. Gaster, "Establishment of laminar boundary layer flow on an aerofoil body," Google Patents, 2008.
- [25] Y. Lin, S. Raghunathan, B. Raghunathan, and S. McIlwain, "Prediction of boundary layer transition on a flat plate subject to surface waviness," *Proc. Inst. Mech. Eng. Part G J. Aerosp. Eng.*, 226(1), pp. 42–54, 2012.
- [26] G. B. Schubauer and P. S. Klebanoff, "Contributions on the mechanics of boundary-layer transition.," NACA TN 3489, 1955.
- [27] F. R. Menter, R. Langtry, S. Völker, and P. G. Huang, "Transition Modelling for General Purpose CFD Codes," *Eng. Turbul. Model. Exp.*, 6, pp. 31–48, 2005.
- [28] F. R. Menter, R. B. Langtry, S. R. Likki, Y. B. Suzen, P. G. Huang, and S. Völker, "A Correlation-Based Transition Model Using Local Variables - Part I: Model Formulation," *J. Turbomach.*, 128(3), p. 413, 2006.
- [29] R. B. Langtry, F. R. Menter, S. R. Likki, Y. B. Suzen, P. G. Huang, and S. Völker, "A Correlation-Based Transition Model Using Local Variables-Part II: Test Cases and Industrial Applications," *J. Turbomach.*, 128(3), p. 423, 2006.
- [30] P. Malan, K. Suluksna, and E. Juntasaro, "Calibrating the Gamma-Re_theta Transition Model for Commercial CFD," in *47th AIAA Aerospace Sciences Meeting including The New Horizons Forum and Aerospace Exposition*, 2009.
- [31] J. Scott, "Aerospaceweb.org | Ask Us - Airliner Takeoff Speeds," 2002. [Online]. Available: <http://www.aerospaceweb.org/question/performance/q0088.shtml>. [Accessed: 30-Aug-2017].

ORCID iD

Dinesh Bhatia  <https://orcid.org/0000-0002-9803-377X>

Guangning Li  <https://orcid.org/0000-0002-2673-9001>



© 2020 by the authors. Licensee SCU, Ahvaz, Iran. This article is an open access article distributed under the terms and conditions of the Creative Commons Attribution-NonCommercial 4.0 International (CC BY-NC 4.0 license) (<http://creativecommons.org/licenses/by-nc/4.0/>).

How to cite this article: Bhatia D., Li G., Sun J., Wang J. Laminar Flow Control and Drag Reduction using Biomimetically Inspired Forward Facing Steps, *J. Appl. Comput. Mech.*, 7(2), 2021, 752–763. <https://doi.org/10.22055/JACM.2020.35082.2557>

